*Int. J. Heat Mass Transfer.* Vol. 30, No. 10, pp. 2097–2113, 1987
Printed in Great Britain

0017–9310/87 $3.00 + 0.00


# Multiple steady states for unicellular natural convection in an inclined porous layer

MIHIR SEN†
Sibley School of Mechanical and Aerospace Engineering, Cornell University, Ithaca, NY 14853, U.S.A.

and

P. VASSEUR and L. ROBILLARD
École Polytechnique, Montréal, P.Q., Canada H3C 3A7

(*Received* 28 *July* 1986 *and in final form* 4 *March* 1987)

**Abstract**—Multiplicity of steady states in natural convection within an inclined porous material with parallel conductive isotherms is investigated. The different steady states are obtained analytically for unicellular convection in thin rectangular porous layers with uniform heating and cooling through opposite walls. The basis of the analytical approximation is an assumption of parallel flow over a large portion of the layer. The two cases of heat fluxes through side and end walls are both calculated and are seen to share some qualitatively similar features. At sub-critical Rayleigh numbers only one steady state exists for any tilt angle. For higher Rayleigh numbers and for small enough inclinations around bottom heating, however, multiple steady states exist, some of which are unstable. Numerical confirmation of the stable analytical results is also presented.

## INTRODUCTION

SOME ASPECTS of natural convection in an inclined fluid saturated porous material and bibliography on the topic can be found in a review by Caltagirone [1] and in other recent papers [2–4]. The point we wish to take up here is that the steady state governing equations for this problem, in common with many other non-linear systems, do not necessarily produce a unique solution under certain boundary conditions and orientations. These multiple steady states usually can be calculated numerically. Theoretical analysis, in general, is difficult and can be carried out only under special simplifying circumstances, one of which will be discussed in this paper. If the multiple states are stable to small perturbations, they may exist in practice. In fact similar behavior has been predicted [5–8], and experimentally observed [9, 10] for flow in natural convection loops and in other related problems. The time-dependent governing equations, on the other hand, can be presumed to have a unique solution as an initial value problem. So when multiple steady states do exist, initial conditions determine the final steady state achieved.

To take a simple case, consider a two-dimensional fluid saturated porous material of any shape. The boundary of the material can be considered impermeable, a fact which translates into a condition on the normal component of the fluid velocity. A prescribed temperature, heat flux or other thermal boundary condition has to be applied as well, its intensity being represented by a Rayleigh number ($R$). One can imagine the application of a symmetrical heating and cooling to a porous material of suitable geometry such that the rest state with conductive heat transfer (temperature governed by the Laplace equation and satisfying the thermal boundary conditions) is a solution of the steady state governing equations. If, however, the thermal boundary conditions or geometry are not symmetric to start with, one can sometimes rotate the porous material in a vertical plane to obtain the rest state. In fact it will *always* be possible to do so if the conductive problem has parallel straight line isotherms which can then be turned to a horizontal position. There will be two such rest states, each with 180° rotation of the porous material with respect to the other. One corresponds to what is physically bottom heating, and the other to top heating. For top heating, an increase in $R$ will not produce any new steady states. For bottom heating there is a critical Rayleigh number ($R_c$) below which the rest state is stable and is the only steady state. For $R > R_c$, however, this rest state is unstable, though it continues to be a solution of the governing equations. Two linearly stable states bifurcate from the rest state at $R = R_c$, each representing convection cells which rotate in opposite directions.

It is not very surprising to have similar behavior for small tilt angles also. Let us measure the inclination of the porous material ($\phi$) counterclockwise from a bottom heated orientation. Then for any $\phi$, however

† Present address: Department of Aerospace and Mechanical Engineering, University of Notre Dame, Notre Dame, IN 46556, U.S.A.

## NOMENCLATURE

| | |
|---|---|
| $A$ | aspect ratio defined as ratio of longer to shorter side |
| $B, B_i$ | integration constants |
| $C$ | constant temperature gradient in $x$-direction |
| $m, n$ | mode numbers |
| $Nu$ | Nusselt number |
| $T$ | temperature |
| $\Delta T$ | temperature difference across layer defined in equation (2) |
| $R$ | Rayleigh number |
| $R_c$ | critical Rayleigh number for zero inclination |
| $R_\phi$ | critical Rayleigh number for non-zero inclination |
| $u$ | velocity in $x$-direction |
| $x, y$ | Cartesian coordinates. |

Greek symbols

| | |
|---|---|
| $\alpha, \beta$ | constants |
| $\theta$ | $y$ dependence of temperature defined in equation (8) |
| $\phi$ | angle of inclination |
| $\phi_a$ | analytical maximum inclination for multiple steady states |
| $\phi_n$ | numerical maximum inclination for multiple steady states |
| $\phi_N$ | inclination for maximum Nusselt number |
| $\phi_S$ | inclination for maximum stream function at center |
| $\phi_T$ | inclination for maximum temperature difference |
| $\psi$ | stream function |
| $\psi_c$ | stream function at center. |

Subscripts and superscripts

| | |
|---|---|
| $'$ | perturbation to steady state |
| 0 | amplitude of perturbation |
| $n$ | mode number. |

small, there is motion and the rest state does not exist as a steady state possibility. Again the number of steady states depends on $R$. For small $R$ only one steady state exists, while for $R > R_\phi$ (where $R_\phi > R_c$), three such states can exist. This behavior has been discussed in the literature for rectangular porous materials with opposite walls at different temperatures. Finite difference calculations were carried out by Moya *et al.* [2]. Some work has also been done by Walch and Dulieu [11] with reasonable qualitative agreement with numerical results. Caltagirone and Bories [4] used a Galerkin method to obtain the three solutions, but their calculations at different aspect ratios seem to imply that the phenomenon would not exist for thin horizontal layers.

The range of steady states which exists is more complex for large values of $R$. For a given set of parameters $R$ and $\phi$, steady cellular convective patterns can exist with different numbers of cells. To facilitate an analytical approach we will consider only the multiplicity of steady states associated with unicellular convection for thin porous layers with a constant heat flux boundary condition. Simplified analytical approximations for this problem were discussed and developed by Vasseur *et al.* [3], who carried out an extensive study of flows which can be started from rest conditions. Good agreement was obtained with the results of numerical integration of the complete partial differential equations. Their theoretical and numerical methods will be used and their analyses extended in the present work to cover the flows which cannot be obtained on starting from rest conditions.

Since we are interested in unicellular convective motions only, the stream function at the center of the layer ($\psi_c$) will be used to identify the sense and magnitude of the circulation. The coordinates are chosen such that counterclockwise (or clockwise) movement will be associated with positive (or negative) $\psi_c$. In addition the terminology followed in ref. [2] will be used for physical coordinate-free interpretation of the convective patterns. Flows which can develop from rest and uniform temperatures as initial conditions will be referred to as 'natural', while those which sometimes exist and which circulate in a direction opposite to this will be called 'antinatural'. These terms are not uniquely associated with the sign of $\psi_c$ and are useful only if we restrict ourselves to unicellular motion. The adjectives 'positive', 'reverse' and 'negative' have also been used in this context [4, 11].

## ANALYSIS

We will consider a rectangular porous layer with its two opposite sides being heated by a uniform heat flux and the other two adiabatic. This falls within the category of cases for which the conductive solution has parallel straight line isotherms. Heating through the side or the end walls represent the two possibilities shown in Figs. 1(a) and (b), respectively, which we shall analyze in turn. The center of the layer will be taken as the origin of coordinates with the $x$- and $y$-directions being along the layer and across it, respectively. For each layer the control parameters will be $R$ and $\phi$. For a parameter set we will determine the distribution of temperature $T$ (to an arbitrary constant) and the stream function $\psi$, using the energy equation and the Darcy law for flow of a large Prandtl

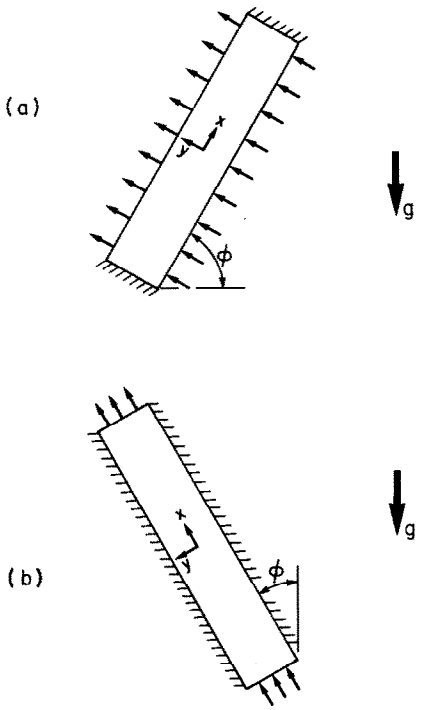


FIG. 1. Definition sketch.

number fluid through a porous medium. All quantities in this text are nondimensionalized as in ref. [3]. The stream function at the center of the layer

$$\psi_c = \psi(0,0) \tag{1}$$

and the temperature difference $\Delta T$ at the $x = 0$ section

$$\Delta T = T(0,-\tfrac{1}{2}) - T(0,\tfrac{1}{2}) \tag{2}$$

will be used to characterize the properties of the convective flows. For side wall heating, the Nusselt number for transverse heat transfer is related to the temperature difference by $Nu = 1/\Delta T$.

We will consider that each layer is long in comparison to its thickness. As a consequence we can assume that for most of the layer the convective flow is parallel to the longer walls. Thus the only component of the velocity is $u$ in the $x$-direction. This approximation, which is justified in greater detail in refs. [3, 12, 13], is the basis of the theoretical analysis in this section. The results to be derived will be called analytical as opposed to those obtained from integration of the partial differential equations discussed in the next section, and which will be referred to as numerical.

We define the Rayleigh number for the porous medium based on the shorter dimension of the layer and the uniform heat flux. The $x$- and $y$-coordinates are nondimensionalized with respect to this distance also. The steady-state energy equation is

$$\nabla^2 T = \frac{\partial \psi}{\partial y}\frac{\partial T}{\partial x} - \frac{\partial \psi}{\partial x}\frac{\partial T}{\partial y}. \tag{3}$$

*Side wall heating*

Consider first the layer shown in Fig. 1(a). From the Darcy law we obtain

$$\nabla^2 \psi = -R\left(\frac{\partial T}{\partial x}\cos\phi - \frac{\partial T}{\partial y}\sin\phi\right) \tag{4}$$

with the boundary conditions

$$\psi = 0, \quad \frac{\partial T}{\partial x} = 0 \quad \text{at} \quad x = \pm\frac{A}{2} \tag{5}$$

$$\psi = 0, \quad \frac{\partial T}{\partial y} = -1 \quad \text{at} \quad y = \pm\tfrac{1}{2} \tag{6}$$

where $A$ is the aspect ratio defined as the ratio of the longer to the shorter sides and taken to be large in this case. The transformation

$$\phi \to -\phi, \psi \to -\psi, \; T \to T, \; x \to -x, \; y \to y \tag{7}$$

does not alter the governing equation nor boundary conditions (3)–(6). This symmetry is evident in opposite quadrants of results such as Fig. 2.

With a parallel flow approximation we can take

$$T = Cx + \theta(y) \tag{8}$$

where $C$ is the constant temperature gradient in the $x$-direction and $\theta$ is the $y$ variation of the temperature. Similar approximations have been used by Walker and Homsy [14] and Bejan and Tien [13] for shallow porous materials with an end-to-end temperature difference. As pointed out in ref. [3] the present approximation coincides with the results given by Bejan [15] for prescribed heat flux conditions using a boundary layer analysis. For the stream function, we have

$$\psi = \psi(y). \tag{9}$$

From equations (3) and (4) we get

$$\frac{\mathrm{d}^2\theta}{\mathrm{d}y^2} - C\frac{\mathrm{d}\psi}{\mathrm{d}y} = 0 \tag{10}$$

$$\frac{\mathrm{d}^2\psi}{\mathrm{d}y^2} - R\sin\phi\frac{\mathrm{d}\theta}{\mathrm{d}y} + RC\cos\phi = 0. \tag{11}$$

An additional constraint is that the heat transported across a transversal section at any $x$ should be zero, so that

$$\int_{-1/2}^{1/2}\left(uT - \frac{\partial T}{\partial x}\right)\mathrm{d}y = 0. \tag{12}$$

There are now three cases to discuss.

(a) $\phi = 0°$ and $180°$ (horizontal layer)

For $\phi = 0°$ the temperature and the stream function distributions from equations (6), (10) and (11) are

$$T = Cx - y\left[1 + \frac{RC^2}{24}(4y^2 - 3)\right] \tag{13}$$

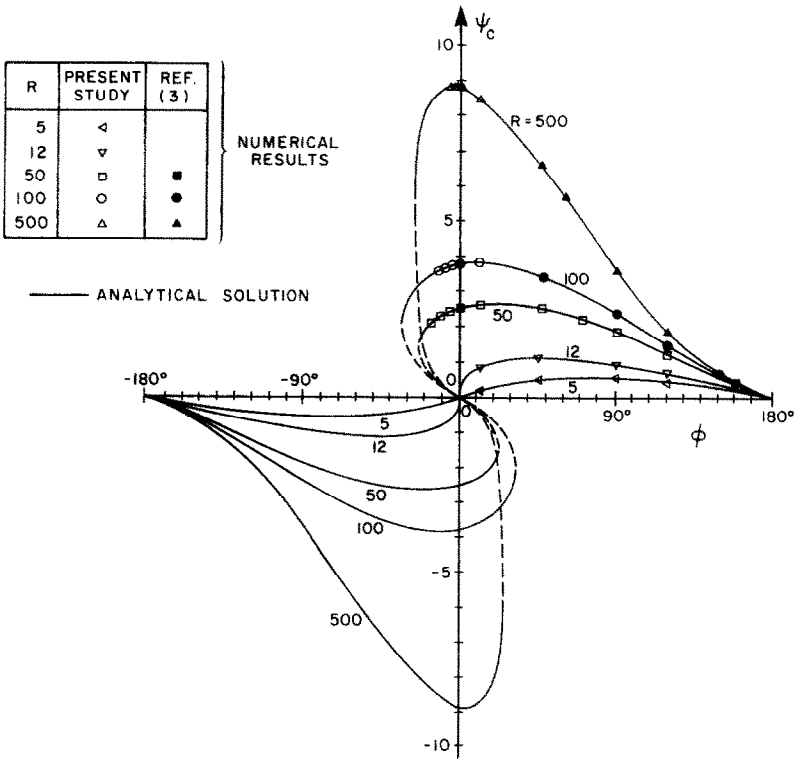


FIG. 2. Stream function at center of layer $\psi_c$ as a function of tilt angle $\phi$ for side wall heating. Broken lines are unstable.

$$\psi = -\frac{RC}{8}(4y^2-1). \tag{14}$$

Substituting in condition (12), we get

$$C(10R-R^2C^2-120)=0 \tag{15}$$

which gives the three solutions

$$C=0 \quad \text{or} \quad C=\pm\frac{1}{R}\sqrt{(10(R-12))}. \tag{16}$$

The last two solutions refer to convective motion and exist only for $R>12$. A value of $R_c=12$ is also reported by Nield [16] as the limit for linear stability of the conductive state with these boundary conditions. For the values of $C$ in equations (16), we also have

$$\psi_c = \frac{RC}{8} \tag{17}$$

$$Nu = \frac{12}{12-RC^2}. \tag{18}$$

For $\phi = 180°$, the only real value of $C$ is zero for which $\psi_c = 0$ and $Nu = 1$.

(b) $C\sin\phi > 0$ (natural flow)

From Fig. 1(a) we can observe that for the inclination shown, $\sin\phi > 0$ and counterclockwise motion would be developed on starting from rest. The $x = A/2$ end would be hotter than the other, and thus $C$ in temperature distribution (8) would be positive. Similarly for $\sin\phi < 0$, flow starting from rest would have a negative $C$. This thus represents natural flow and was discussed thoroughly in ref. [3] with the following results:

$$\psi_c = \frac{B}{C}\left[1-\cosh\frac{\alpha}{2}\right] \tag{19}$$

$$Nu = -\frac{\alpha}{2B\sinh\frac{\alpha}{2}+\alpha C\cot\phi} \tag{20}$$

where the constants are determined from

$$\alpha^2 = RC\sin\phi \tag{21}$$

$$B = -\frac{1+C\cot\phi}{\cosh\frac{\alpha}{2}} \tag{22}$$

$$C-\frac{B^2}{2C}\left(\frac{\sinh\alpha}{\alpha}-1\right) - B\cot\phi\left[\cosh\frac{\alpha}{2}-\frac{2}{\alpha}\sinh\frac{\alpha}{2}\right]=0. \tag{23}$$

(c) $C\sin\phi < 0$ (antinatural flow)

The circulation is now in an opposite sense. In Fig. 1(a), for instance, antinatural flow corresponds to a

clockwise rotation. An analysis similar to the above can be carried out such that we obtain

$$\psi_c = \frac{B}{C}\left[1-\cos\frac{\beta}{2}\right] \tag{24}$$

$$Nu = -\frac{\beta}{2B\sin\frac{\beta}{2}+\beta C\cot\phi} \tag{25}$$

with the constants being calculated from

$$\beta^2 = -RC\sin\phi \tag{26}$$

$$B = -\frac{1+C\cot\phi}{\cos\frac{\beta}{2}} \tag{27}$$

$$C-\frac{B^2}{2C}\left(\frac{\sin\beta}{\beta}-1\right)-B\cot\phi\left[\cos\frac{\beta}{2}-\frac{2}{\beta}\sin\frac{\beta}{2}\right]=0. \tag{28}$$

Strictly speaking, all three cases above are covered by the set of equations (19)–(23) or (24)–(28) which are really equivalent if we put $\alpha = i\beta$. However, if real numbers are to be handled it is easier if the problem is split up into the three cases as is done here. Moreover, the present procedure has the advantage that the difference between the natural and antinatural states are brought out. A Newton–Raphson procedure can be used to solve the simultaneous transcendental equations (21)–(23) and (26)–(28). Since some of the roots are near each other and slopes are high at the roots, it helps to initially identify their location and number by plotting functions (23) and (28).

*End wall heating*

We refer now to Fig. 1(b). The equation for the stream function is

$$\nabla^2\psi = R\left(\frac{\partial T}{\partial x}\sin\phi+\frac{\partial T}{\partial y}\cos\phi\right). \tag{29}$$

The boundary conditions are

$$\psi = 0, \quad \frac{\partial T}{\partial x} = -1 \quad \text{at} \quad x = \pm\frac{A}{2} \tag{30}$$

$$\psi = 0, \quad \frac{\partial T}{\partial y} = 0 \quad \text{at} \quad y = \pm\tfrac{1}{2}. \tag{31}$$

Symmetry is evident by the invariance of equations (3) and (29)–(31) under the transformation

$$\phi \to -\phi, \quad \psi \to -\psi, \quad T \to T, \quad x \to x, \quad y \to -y. \tag{32}$$

All the heat is transported in the $x$-direction so that at any $x$, we have

$$\int_{-1/2}^{1/2}\left(uT-\frac{\partial T}{\partial x}\right)dy = 1. \tag{33}$$

With the parallel flow approximations (8) and (9), equation (29) becomes

$$\frac{d^2\psi}{dy^2} - R\cos\phi\frac{d\theta}{dy} - RC\sin\phi = 0. \tag{34}$$

Equation (10) remains the same.

The sign of $C\cos\phi$ no longer distinguishes the natural from the antinatural circulation. However, once again for simplicity we analyze the following three cases.

(a) $\phi = 0°$ and $180°$ (vertical layer)

For $\phi = 0°$ the temperature and stream function are

$$T = Cx + \frac{B_1}{\alpha}\sin(\alpha y) - \frac{B_2}{\alpha}\cos(\alpha y) \tag{35}$$

$$\psi = \frac{B_1}{C}\cos(\alpha y) + \frac{B_2}{C}\sin(\alpha y) + B_3 \tag{36}$$

where

$$\alpha^2 = -RC. \tag{37}$$

Applying the temperature boundary condition (31), two equations are obtained. These can have the trivial solution which leads to the conductive state

$$T = -x, \quad \psi = 0. \tag{38}$$

This is the only state obtained by setting $\phi = 0$ in equations (49)–(53) or (54)–(58) below. Non-trivial solutions are possible when the determinant of the system is zero. This gives $\sin\alpha = 0$, from which $\alpha = n\pi$, $n = 1, 2, 3, \ldots$

For the odd modes $n = 1, 3, 5, \ldots$, we obtain on using equations (31), (33), and (35)–(37)

$$T^{(n)} = -\frac{n^2\pi^2}{R}x + \frac{B_1^{(n)}}{n\pi}\sin(n\pi y) \tag{39}$$

$$\psi^{(n)} = -\frac{B_1^{(n)}R}{n^2\pi^2}\cos(n\pi y) \tag{40}$$

where

$$B_1^{(n)} = \pm\frac{n\pi}{R}\sqrt{(2(R-n^2\pi^2))}. \tag{41}$$

The stream function at the center is

$$\psi_c^{(n)} = \mp\frac{1}{n\pi}\sqrt{(2(R-n^2\pi^2))} \tag{42}$$

and the temperature difference across the central section of the layer is

$$\Delta T^{(n)} = \mp\frac{2}{R}(-1)^{(n-1)/2}\sqrt{(2(R-n^2\pi^2))}. \tag{43}$$

Only the first mode $n = 1$ is unicellular. All these odd modes are present in equations (49)–(53) as $\phi \to 0$.

For the even modes $n = 2, 4, 6, \ldots$ in a similar manner

$$T^{(n)} = -\frac{n^2\pi^2}{R}x - \frac{B_2^{(n)}}{n\pi}\cos(n\pi y) \tag{44}$$

$$\psi^{(n)} = -\frac{B_2^{(n)} R}{n^2\pi^2}\sin(n\pi y) \tag{45}$$

$$B_2^{(n)} = \pm\frac{n\pi}{R}\sqrt{(2(R-n^2\pi^2))} \tag{46}$$

$$\psi_c^{(n)} = 0 \tag{47}$$

$$\Delta T^{(n)} = 0. \tag{48}$$

All even modes give multicellular motion.

The lowest $R$ at which convective motion exists is given by the unicellular motion which from equation (41) is seen to be $\pi^2$. A linear stability analysis of the conductive state is outlined in the Appendix, confirming the value of $R_c = \pi^2$ for these boundary conditions.

For $\phi = 180°$ only the conductive mode exists.

(b) $C\cos\phi > 0$

This case was analyzed in ref. [3]. The stream function at the center is

$$\psi_c = \frac{B}{C}\left[1-\cosh\frac{\alpha}{2}\right]. \tag{49}$$

The temperature difference at $x = 0$ is

$$\Delta T = -\frac{2B}{\alpha}\sinh\frac{\alpha}{2} + C\tan\phi \tag{50}$$

where the constants are determined from

$$\alpha^2 = RC\cos\phi \tag{51}$$

$$B = \frac{C\tan\phi}{\cosh\dfrac{\alpha}{2}} \tag{52}$$

$$1+C-\frac{B^2}{2C}\left(\frac{\sinh\alpha}{\alpha}-1\right) + B\tan\phi\left[\cosh\frac{\alpha}{2}-\frac{2}{\alpha}\sinh\frac{\alpha}{2}\right] = 0. \tag{53}$$

(c) $C\cos\phi < 0$

The corresponding relations are now

$$\psi_c = \frac{B}{C}\left[1-\cos\frac{\beta}{2}\right] \tag{54}$$

$$\Delta T = -\frac{2B}{\beta}\sin\frac{\beta}{2} + C\tan\phi \tag{55}$$

$$\beta^2 = -RC\cos\phi \tag{56}$$

$$B = \frac{C\tan\phi}{\cos\dfrac{\beta}{2}} \tag{57}$$

$$1+C-\frac{B^2}{2C}\left(\frac{\sin\beta}{\beta}-1\right) + B\tan\phi\left[\cos\frac{\beta}{2}-\frac{2}{\beta}\sin\frac{\beta}{2}\right] = 0. \tag{58}$$

Once again equations (49)–(53) and (54)–(58) are identical if we put $\alpha = i\beta$.

## NUMERICAL PROCEDURE

A finite difference procedure was used for numerical integration of the time-dependent governing equations. The temperature distribution was obtained from the unsteady form of the energy equation (3) using the alternating direction implicit (ADI) method of Peaceman and Rachford [17]. Using this temperature, the stream function was determined from equation (4) or (29) using successive over-relaxation (SOR), before returning to the energy equation. Integration in time was continued to steady state. Trial calculations were necessary in order to optimize computation time and accuracy. A $51 \times 51$ grid was found to accurately model the flow fields described in the numerical results. For instance, with $R = 250$, $\phi = 90°$ and $A = 4$, Nusselt numbers of 4.59 and 4.54 were obtained with $51 \times 51$ and $81 \times 81$ meshes, respectively. To have an additional check on the results, an energy balance was used for the system. The heat transfer through each $y =$ constant plane was evaluated for $-1/2 < y \leqslant 1/2$ and compared to the heat input at $y = -1/2$. For most of the results reported here, the energy balance was satisfied to within 1–2%. Other details of the numerical scheme are given in refs. [3, 12].

A remark must be made with regard to the numerical procedure which would apply also to other cases where any integration in time is used to solve a problem with multiple linearly stable steady states. Each of these states has its own basin of attraction and only initial conditions within this basin will evolve to the desired steady state within it. Thus, initial conditions have to be chosen carefully for each numerical run. There are two special cases for which non-rest initial conditions are necessary. First, for a nearly horizontal layer heated through the side walls, one has to start from conditions corresponding to a tilted layer to obtain unicellular motion as was done in ref. [3]. Second, to obtain antinatural flows the technique used in refs. [2, 11] was to begin from a state corresponding to the natural circulation direction followed by a small numerical change in the tilt angle.

The procedure outlined above has some limitations which would be applicable to other numerical methods which could have been used. Unstable flows, even though analytically predicted as solutions of the steady-state equations, cannot be obtained. However, if the stream function and temperature fields converge to a steady state, this itself is evidence of asymptotic stability to small perturbations. If more than one such linearly stable state coexists, it is evident that none of them can be asymptotically stable to large enough perturbations which could take the instantaneous state out of the respective basin of attraction. This becomes important in the determination of antinatural states near the turning point

bifurcation represented by the boundary of existence of these states in parameter space. Here the steady state nears the boundary of its own basin of attraction. If suitable initial conditions are not chosen, the numerical solution evolves to some other state which could be the natural state or multicellular flow. Under such conditions, one has to make a large number of computations with very small rotations of the layer after each computation and use the previous state as initial condition to assure convergence to the desired antinatural state. Even if such a linearly stable steady state exists, the procedure may become prohibitively time consuming after a point.

## ANALYTICAL AND NUMERICAL RESULTS

We will present results obtained from the analyses. Comparison will also be made between the theoretical analysis and numerical calculations. The latter were all for a cavity with aspect ratio $A = 4$, since it was demonstrated in ref. [3] that near this value the stream function and temperature fields over the central part of the porous material become independent of $A$. Results for the natural flows have been previously treated and will be included here for completeness but not discussed in much detail. The presentation will be separated into the two heating modes for the porous layer.

*Side wall heating*

The stream function at the center $\psi_c$ is one indicator of the strength of the circulation due to convection. Figure 2 shows $\psi_c$ as a function of $\phi$ for different $R$ obtained from the analysis. The first and third (or second and fourth) quadrants represent the natural (or antinatural) flows. In the first (or third) quadrant we have positive (or negative) $\psi_c$ which represents counterclockwise (or clockwise) motion. For $R < R_c$ ($R_c = 12$ in this case), the curve is single valued. But for $R = R_c$, a point of inflexion is developed at the origin where it is tangent to the $\phi = 0°$ axis. For $R > R_c$ and for small tilt angles, three values of $\psi_c$ are possible. Verification of the results of analysis by numerical computation is also indicated on the upper half of the figure. Some of the values for the natural flows are from ref. [3] as indicated. Table 1 for the antinatural flows gives a detailed idea of the degree of agreement (better than 1% for $\psi_c$) that is obtained between the two methods. Stability characteristics can also be deduced from the numerical information. For some values of $R$, part of the outer branch covering both natural as well as antinatural states is stable. At high enough $R$ all of it becomes unstable. The inner antinatural branch is always unstable and is shown by broken lines. Strictly speaking, instability has been analytically shown only for one point on this branch [16], which is the conductive steady state represented by the origin.

Analysis indicates that the multiple steady states exist for tilt angles $-\phi_a < \phi < \phi_a$, where $\phi_a$ is shown in Fig. 3. $\phi_a$ rises to a maximum of 35° and then goes up and down around 30°. Numerically, however, it was possible to get multiple steady states only for $-\phi_n < \phi < \phi_n$ (with $\phi_n < \phi_a$) where $\phi_n$ is also shown in Fig. 3. Even with great care in the selection of initial conditions and using increments of half a degree, only natural unicellular or multicellular motions are obtained in the $|\phi_n| < |\phi| < |\phi_a|$ range. The reason for the difference between $\phi_a$ and $\phi_n$ can only be speculated at this point. It is similar to that observed in natural circulation loop experiments in ref. [10]. All that can be said is that it is consistent with the instability of the antinatural unicellular motion which becomes an increasingly important factor for large $R$. $\phi_n$ would then be a stability limit as opposed to $\phi_a$ which is an existence limit.

Figure 4 shows $Nu$ as a function of tilt angle for different $R$. The antinatural flows are shown with broken lines. Numerically obtained values are also indicated. Comparison of analytical and numerical Nusselt numbers for antinatural flows is also included in Table 1. Agreement is better at low Rayleigh numbers and inclinations.

The maximum values of $Nu$ and $\psi_c$ occur at $\phi = \phi_N$ and $\phi = \phi_S$, respectively, where $\phi_N$ and $\phi_S$ are shown in Fig. 5. For small $R$ the temperature field is conduction dominated. The largest buoyancy force and circulation is with inclination near 90° since the temperature gradient must be horizontal. The large circulation reduces $\Delta T$ and increases $Nu$ as expected. Thus the maximum $Nu$ inclination correlates well with the maximum $\psi_c$ inclination for small $R$. For large $R$ the difference between the two curves is striking. The maximum $\psi_c$ occurs at smaller inclinations and for $R > 225$ even shifts to the antinatural side. $\phi_N$ however, turns slowly towards 90°. The temperature field is convection dominated for large $R$. Again the temperature gradient should be horizontal for maximum circulation, this being now near 0°. However, increasing the circulation does not necessarily increase $Nu$ substantially; in fact for $\phi = 0°$, $Nu \to 6$ asymptotically as $R \to \infty$ [3]. In relation to this it should also be noted that for small $\alpha$ in equations (19)–(23), i.e. small $R$ and $\cot\phi$ of order 1 or less, the velocity profiles $u(y)$ are similar and scale only with $\psi_c$. The temperature profiles also scale with $\Delta T$. For large $\alpha$, however, $\psi_c$ alone does not determine the velocity field, nor $\Delta T$ the temperature field. Thus in the latter case, some quantity such as the volumetric average of the kinetic energy [18] should perhaps be used to measure the global strength of the circulation, or some other combination of the present control parameters chosen.

Figure 6(a) shows $\psi_c$ as a function of $R$ for $\phi = 0°$, 5° and 10°. For the horizontal layer there is no motion possible up to the critical Rayleigh number $R_c$, where a bifurcation into two counterrotating convection states occurs. The diagram changes considerably for any inclination, however small. For positive inclinations shown, the upper half represents natural cir-

Table 1. Analytical and numerical antinatural Nusselt number and stream function at center for side wall heating

| $R$ | $\phi$ | $\psi_c$ Analytical | $\psi_c$ Numerical | $Nu$ Analytical | $Nu$ Numerical |
|---|---|---|---|---|---|
| 25 | −5 | 1.27 | 1.28 | 1.625 | 1.618 |
| | −6 | 1.23 | 1.24 | 1.589 | 1.589 |
| | −7 | 1.19 | 1.20 | 1.549 | 1.551 |
| 50 | −5 | 2.35 | 2.36 | 2.617 | 2.617 |
| | −10 | 2.23 | 2.24 | 2.480 | 2.481 |
| | −11 | 2.21 | 2.21 | 2.449 | 2.449 |
| | −12 | 2.18 | 2.18 | 2.415 | 2.416 |
| | −13 | 2.14 | 2.16 | 2.380 | 2.381 |
| | −14 | 2.11 | 2.13 | 2.343 | 2.352 |
| 72 | −5 | 2.99 | 3.00 | 3.162 | 3.160 |
| | −10 | 2.89 | 2.90 | 3.028 | 3.027 |
| | −11 | 2.87 | 2.88 | 2.999 | 2.997 |
| | −12 | 2.85 | 2.85 | 2.968 | 2.965 |
| | −13 | 2.82 | 2.83 | 2.935 | 2.933 |
| | −14 | 2.79 | 2.80 | 2.902 | 2.899 |
| | −15 | 2.76 | 2.77 | 2.867 | 2.863 |
| 100 | −5 | 3.65 | 3.66 | 3.628 | 3.627 |
| | −10 | 3.56 | 3.57 | 3.485 | 3.483 |
| | −11 | 3.54 | 3.55 | 3.454 | 3.452 |
| | −12 | 3.52 | 3.53 | 3.422 | 3.422 |
| | −13 | 3.50 | 3.51 | 3.389 | 3.384 |
| | −14 | 3.47 | 3.48 | 3.354 | 3.349 |
| 150 | −5 | 4.60 | 4.61 | 4.133 | 4.135 |
| | −10 | 4.53 | 4.55 | 3.962 | 3.965 |
| | −11 | 4.51 | 4.53 | 3.925 | 3.929 |
| | −12 | 4.49 | 4.51 | 3.887 | 3.893 |
| | −13 | 4.47 | 4.49 | 3.848 | 3.855 |
| | −14 | 4.45 | 4.45 | 3.808 | 3.764 |
| 500 | −5 | 8.79 | 8.79 | 4.997 | 5.110 |
| | −6 | 8.79 | 8.79 | 4.922 | 5.032 |
| | −7 | 8.79 | 8.79 | 4.845 | 4.952 |
| | −8 | 8.79 | 8.79 | 4.768 | 4.936 |

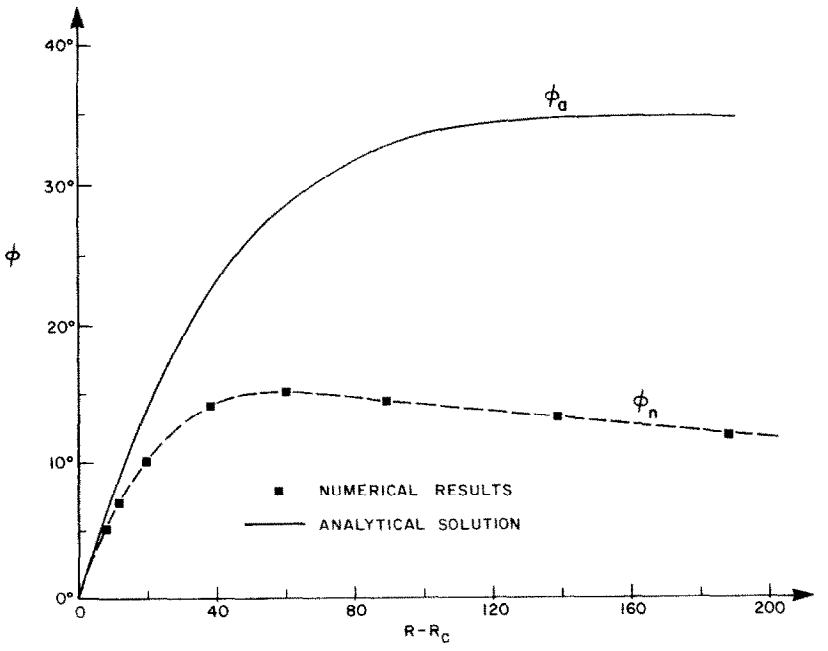


FIG. 3. Range of tilt angles for multiple steady states with side wall heating. $\phi_a$ is analytical and $\phi_n$ is numerical.

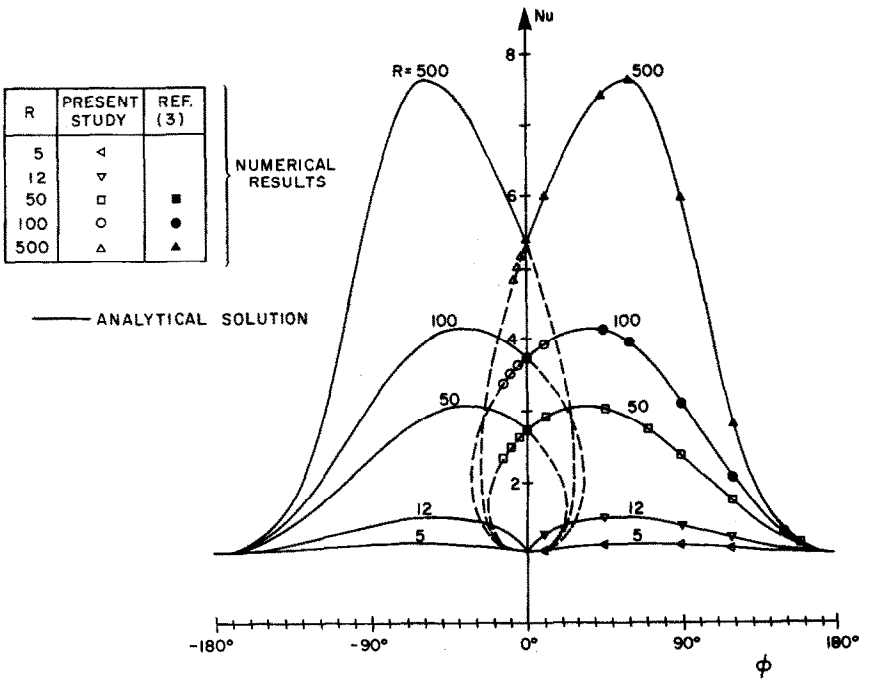


FIG. 4. Nusselt number $Nu$ as a function of tilt angle $\phi$ for side wall heating. Broken lines are antinatural circulations.

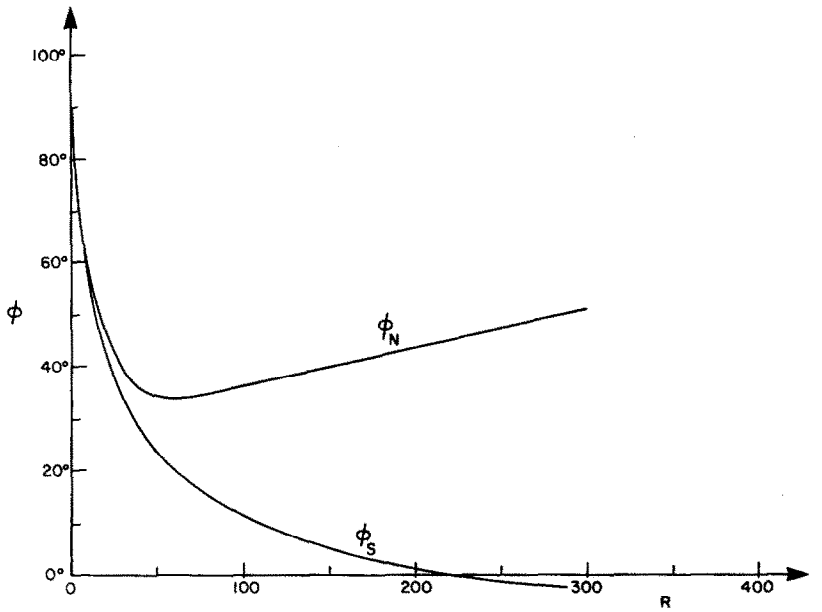


FIG. 5. Tilt angle for maximum stream function $\phi_S$ and for maximum Nusselt number $\phi_N$ for side wall heating.

culation while the lower half is antinatural. The unstable part of the antinatural branch is indicated by broken lines. Numerical confirmation of the stable solutions is also indicated. Heating from zero temperature rest conditions would be equivalent to gradually increasing $R$ from zero. Any inclination would bias the convection towards the natural state. The antinatural state can be reached only through initial conditions different from rest and exists only if $R > R_\phi$. $R_\phi$ can also be measured from Fig. 3 by reading off the Rayleigh number for a given inclination on the ordinate. In Fig. 6(a), $R_\phi$ acts as a critical Rayleigh

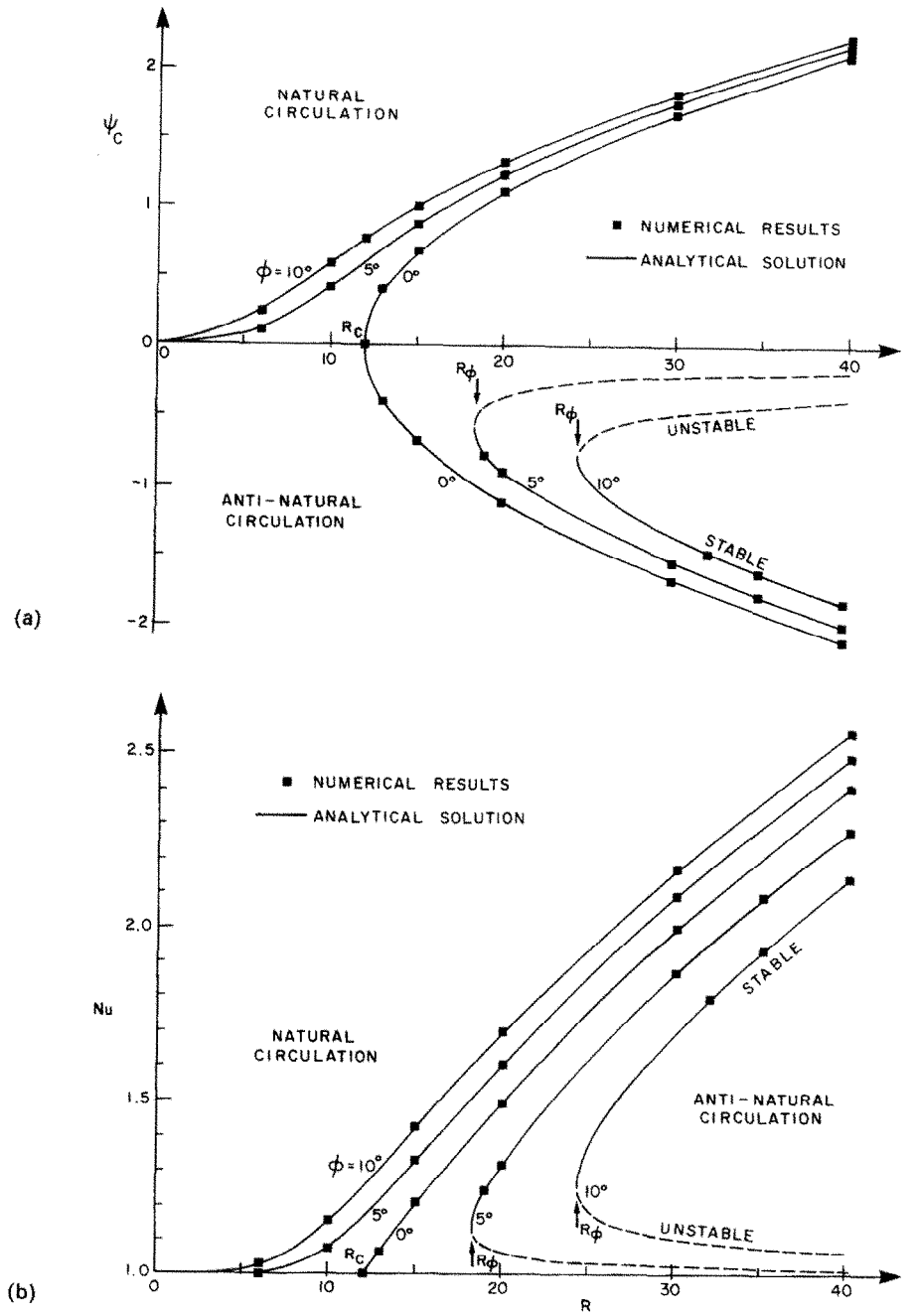


FIG. 6. (a) Stream function at center and (b) Nusselt number $Nu$ as a function of Rayleigh number $R$ for side wall heating with tilt angle $\phi = 0°$, 5° and 10°. Broken lines are unstable. $R_c$ and $R_\phi$ are critical Rayleigh numbers.

number for the inclined layer in the sense that $R_c$ and $R_\phi$ can both be defined as the smallest Rayleigh number at which multiple steady states appear, the first for zero inclination and the second for an inclined layer. However, $R_c$ also represents the smallest Rayleigh number at which convective motion first appears, while $R_\phi$ does not. The corresponding Nusselt number is shown in Fig. 6(b). For negative inclinations, Fig. 6(b) is not altered, though the sign of $\psi_c$ in Fig. 6(a) changes. Thus if one starts from initial conditions corresponding to the natural state for $\phi = 5°$, for instance, one is relatively close to the anti-natural state for $\phi = -5°$. This is the basis of the numerical procedure for obtaining the antinatural solutions.

The numerical method permits a detailed picture of the streamlines and isotherms. As an example, Figs. 7(a) and (b) show these for the natural and anti-

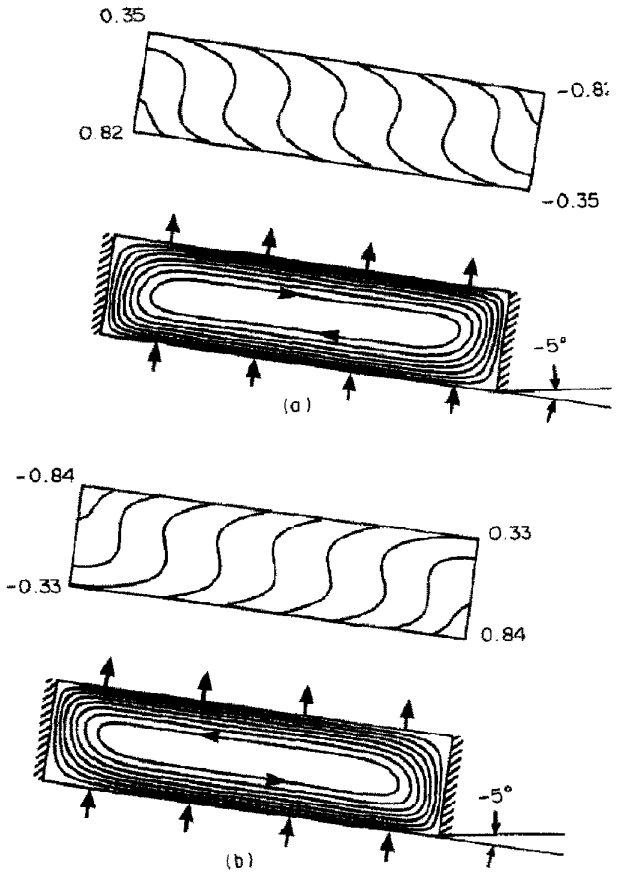


FIG. 7. Isotherms and streamlines for side wall heating corresponding to $R = 100$ and $\phi = -5°$: (a) natural, $\psi_c = -3.75$; (b) antinatural, $\psi_c = 3.66$. Corner temperatures are noted.

natural stable flows that co-exist for $R = 100$, $\phi = -5°$. For reference the maximum and minimum temperatures at each corner of the rectangle are also indicated. The approximate validity of our basic assumptions of parallel flow in the central region is evident. The details of transition from an antinatural unicellular pattern is illustrated by Fig. 8. On increasing the tilt slowly from $-14°$ to $-17°$, the change is first to an intermediate multicellular pattern and then to natural unicellular motion. Each one of the states shown is stable to small temperature and velocity perturbations. Loss of stability of the antinatural convection pattern to increasing tilt in this case is thus by exchange of stability to the multicellular stable state.

*End wall heating*

Results similar to the previous case are obtained for the stable outer states. Figure 9 shows $\psi_c$ for different $\phi$ and $R$. $C\cos\phi$ is negative for $-90° < \phi < 90°$ and positive outside. As far as the outer branches are concerned, the first and third quadrants again represent natural flow since they can be started from rest, while the other two quadrants are antinatural. In the outer branch, due to instability it was possible at $R = 500$ to obtain neither unicellular flow for $\phi = 0°$ nor antinatural flows. In fact even unicellular natural flows for non-zero $\phi$ were difficult to simulate numerically for this $R$. In comparison to side wall heating, the inner branches are much more intricate. For $R = 500$, there are nine steady states at zero $\phi$, while $R = 100$ has five. The values at the intersections as well as their number, can be determined from equation (42). At each critical $R$, the $\psi_c$ vs $\phi$ curve becomes tangent to the ordinate at the origin. Numerical verification of some of the analytical results is also provided on the figure. Table 2 shows the results for the antinatural flows for $R = 100$. Once again agreement is very good.

As pointed out in ref. [3], the Nusselt number for heat transfer between the non-adiabatic walls is very much dependent on the flow pattern in the end regions and thus cannot be suitably predicted here. However, $\Delta T$ can be used as an indicator of the transversal temperature distribution and is shown in Fig. 10. Since the heat transfer is globally in the $x$-direction, $\Delta T$ is relatively small and varies little with $R$. In the figure the central part of the $R = 500$ curve near the origin has been omitted for clarity. The shape of the

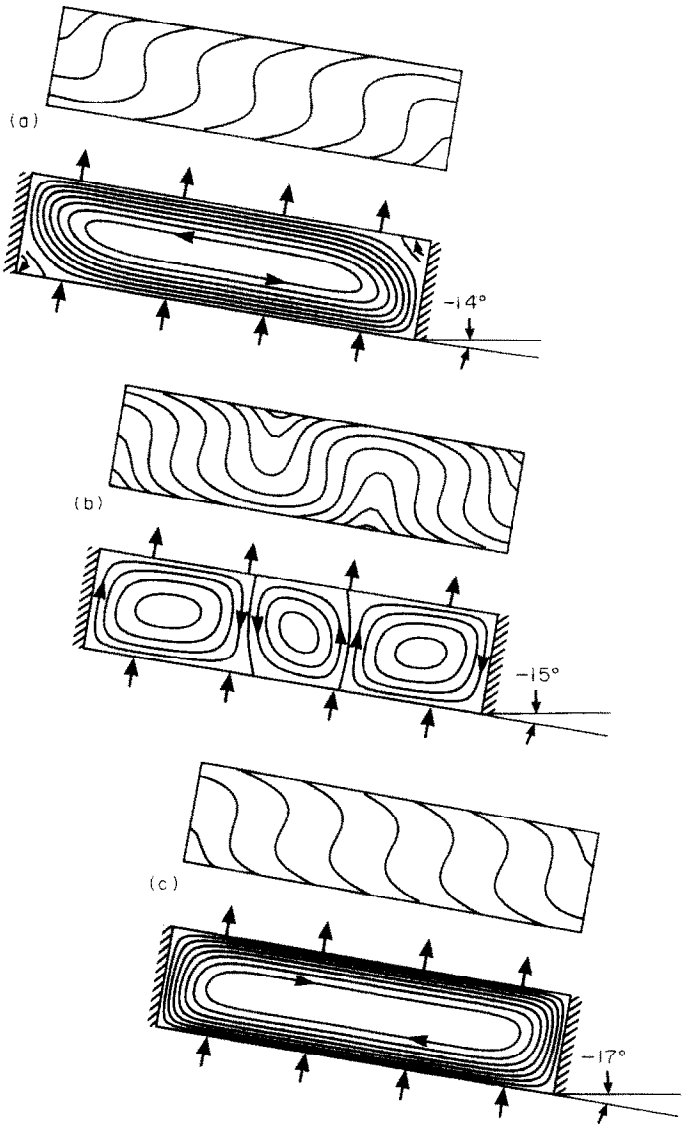


FIG. 8. Isotherms (above) and streamlines (below) for (a) antinatural, $\phi = -14°$, (b) multicellular, $\phi = -15°$, and (c) natural, $\phi = -17°$.

Table 2. Analytical and numerical antinatural temperature difference and stream function at center for end wall heating

| $R$ | $\phi$ | $\psi_c$ Analytical | $\psi_c$ Numerical | $\Delta T$ Analytical | $\Delta T$ Numerical |
|---|---|---|---|---|---|
| | −1 | 4.26 | 4.29 | 0.269 | 0.271 |
| | −2 | 4.25 | 4.28 | 0.270 | 0.272 |
| | −3 | 4.24 | 4.26 | 0.271 | 0.272 |
| | −4 | 4.22 | 4.25 | 0.271 | 0.273 |
| | −5 | 4.21 | 4.23 | 0.272 | 0.274 |
| | −6 | 4.19 | 4.22 | 0.273 | 0.275 |
| 100 | −7 | 4.17 | 4.20 | 0.274 | 0.275 |
| | −8 | 4.15 | 4.18 | 0.275 | 0.276 |
| | −9 | 4.14 | 4.17 | 0.276 | 0.277 |
| | −10 | 4.12 | 4.15 | 0.277 | 0.278 |
| | −11 | 4.09 | 4.13 | 0.278 | 0.279 |
| | −12 | 4.07 | 4.11 | 0.279 | 0.280 |
| | −13 | 4.05 | 4.09 | 0.280 | 0.282 |

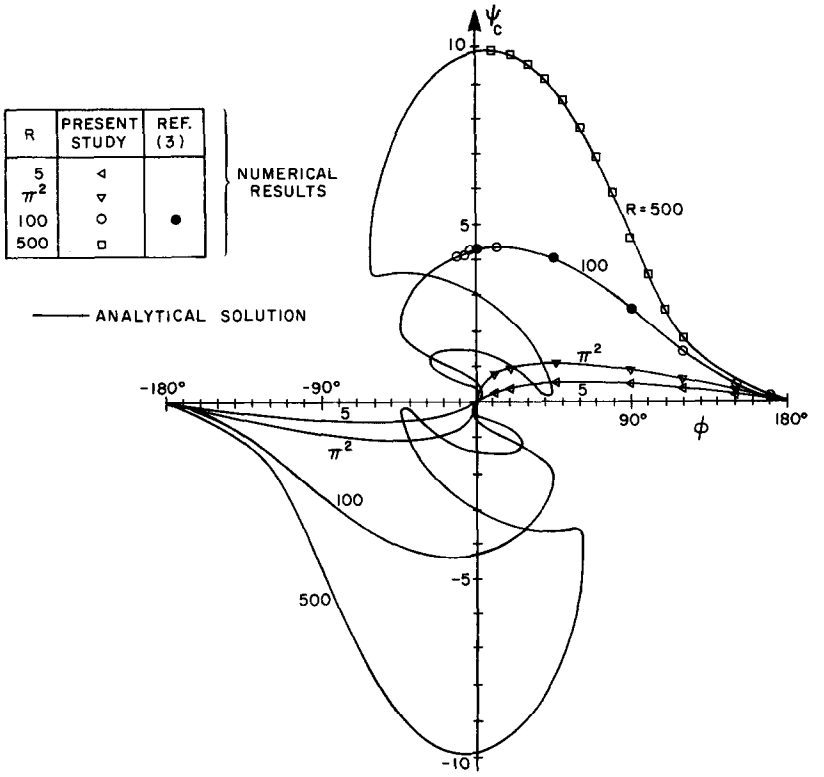


FIG. 9. Stream function at center of layer $\psi_c$ as a function of tilt angle $\phi$ for end wall heating.

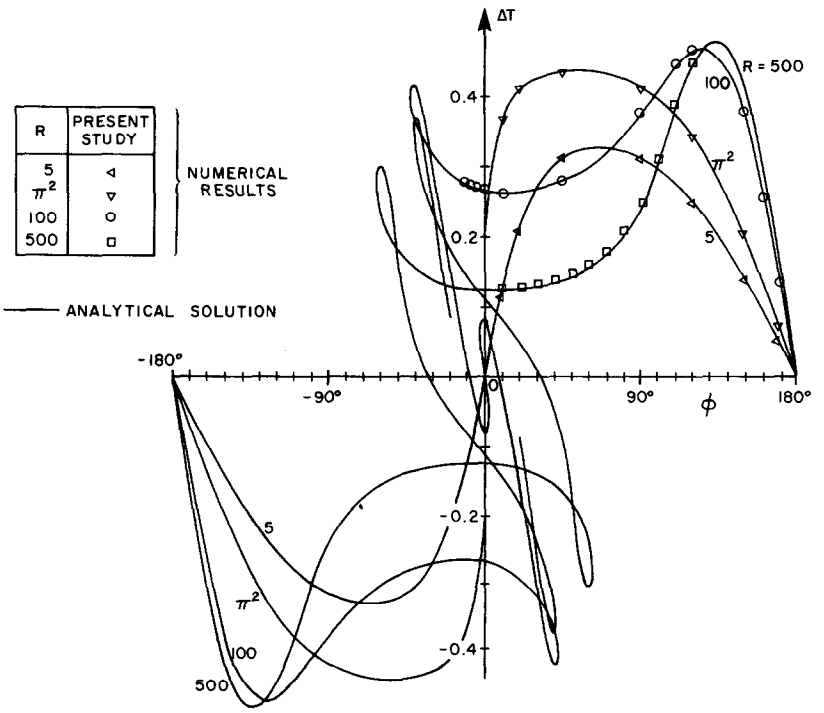


FIG. 10. Temperature difference $\Delta T$ as a function of tilt angle for end wall heating. Central part of $R = 500$ curve is omitted.

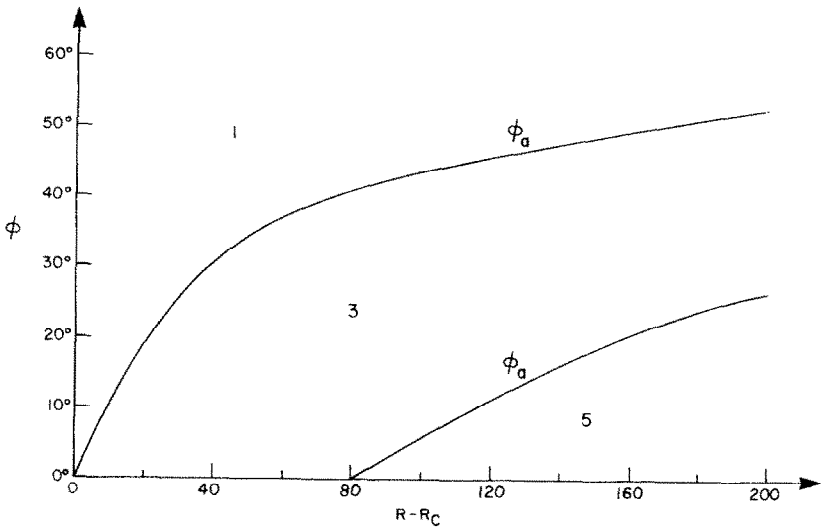


FIG. 11. Range of tilt angles for multiple steady states with end wall heating calculated analytically. The number of possible modes is indicated.

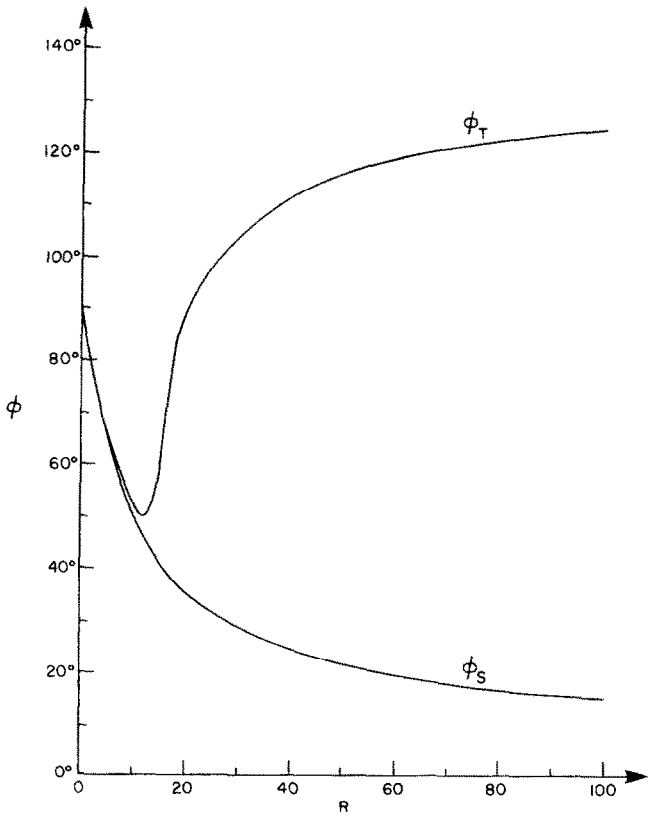


FIG. 12. Tilt angle for maximum stream function $\phi_S$ and for maximum temperature difference $\phi_T$ for end wall heating.

curves in the antinatural part are quite different from what they would be for side wall heating as deduced from Fig. 4.

The range of inclinations $-\phi_a < \phi < \phi_a$ over which multiple states exist analytically is shown in Fig. 11. In the range of parameters shown the lines separate regions with one, three or five steady states. The critical $R$ values at which they meet the abscissa correspond to those from equation (41), or equivalently from the Appendix, equation (A7) with the wave number $m = 0$.

Figure 12 shows the inclination $\phi_S$ at which the maximum stream function occurs. Like in side wall heating, the highest circulation is obtained for infinitesimal $R$ with the temperature gradient horizontal. However, this is not so for finite $R$, even though the

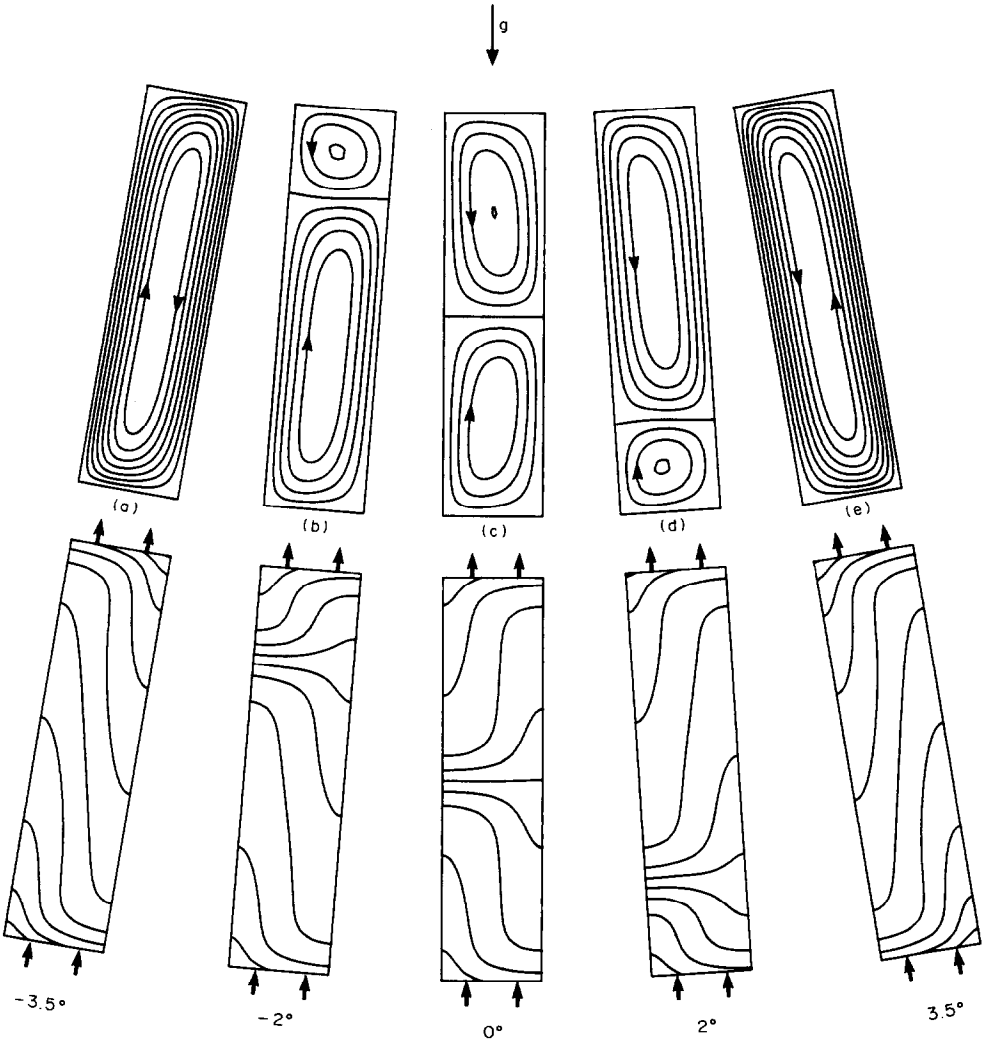


FIG. 13. Isotherms (below) and streamlines (above) for end wall heating for $R = 100$ around 0°.

antinatural states are never stronger than the natural ones in this case. Figure 12 also shows the angle $\phi_T$ at which the maximum value of $\Delta T$ occurs, being very similar to $\phi_S$ only for small $R$.

The range of possible solutions is much larger if multicellular patterns are also included. Figure 13 shows one kind of stable bicellular convection obtained numerically for $R = 100$. With $\phi$ changing from zero in both the positive and negative directions, the cell in the natural circulation direction in each case grows rapidly. The cell rotating in an opposite direction is thus eliminated at a relatively small angle. It should also be remarked that for large enough aspect ratios, two or more cells may exist with parallel flow except in the end and intercellular regions.

## DISCUSSION AND CONCLUSIONS

Multiplicity of linearly stable steady states exists for natural convection in porous materials. Though some of these are numerically shown to be multicellular, we have simplified matters by concentrating on unicellular circulation, since that allows approximate analytical calculation. With geometry and thermal boundary conditions such that conductive isotherms are straight lines, certain generalizations can be made. Multiple steady states can be obtained for super-critical Rayleigh numbers and for small tilt angles around the bottom heated orientation. Moreover, the shape of the stable outer part of the curves in Figs. 2 and 9 are similar though specific values are not.

Constant temperatures applied to the opposite sides of a square geometry in ref. [2] afforded an earlier example of the multiplicity of steady states. In the present work we have analytically investigated a porous layer with uniform heat flux. Both side wall and end wall heating gave qualitatively similar results. With numerical integration of the complete partial differential equations we have been able to confirm the stable analytical solutions, obtaining very good agreement between them. It can be pointed out that

the results in ref. [2] were entirely numerically obtained.

Antinatural circulation is not difficult to understand in physical terms. In Figs. 1(a) and (b), for instance, this would be clockwise flow. Consider a parcel of cold fluid starting from the rightmost corner of each figure. It gets hotter as it comes down a heated wall. It moves along the adiabatic wall essentially without change in temperature and then, being hot still, rises along the cooled wall. When it reaches the rightmost corner it is once again cold so that it descends. The corner temperatures marked in Fig. 7 reflect this pattern. Mathematically, multiplicity is the result of nonlinearity of heat convection, which is represented by the first term on the right-hand side of equation (3) and the first terms of the integrands of equations (12) and (33).

A numerical procedure based on time integration of the governing equations not only confirms the existence of a steady state if convergence is reached, but also assures its linear asymptotic stability. Thus at least two stable flows, one natural and the other antinatural, were calculated for certain parameter values. However, numerical computation of the antinatural states in ref. [2] as well as here is increasingly difficult as one nears the turning point, possibly due to flow instability. The theoretical analysis presents no such difficulties and provides information with respect to the range of angles for multiple steady states. Among the two types of layers investigated here we find that tall vertical layers have a wider range as compared to shallow horizontal ones.

Critical Rayleigh numbers obtained here for the onset of convection at zero tilt angles are exactly equal to those determined from linear stability analyses for the two layers studied. Numerical computations have also conformed to these values as expected. The basic reason for this agreement is that both layers become unstable at zero wave numbers for which the present analysis is exact.

Multiplicity of steady states in this work closely parallels that of natural convection in a closed circulation loop [8, 10]. The relation is not fortuitous but due to fundamental similarity in the underlying physics. In fact, in principle it should be possible to generalize some of the qualitative aspects presented in this paper to include other natural convection flows in enclosures and porous media with parallel conductive isotherms.

*Acknowledgements*—The authors acknowledge support from the U.S. National Science Foundation under Grant MEA 8401489 and from the Natural Sciences and Engineering Reserch Council of Canada through Grants A-9201 and A-4197. We are also grateful to the École Polytechnique which provided time on an IBM 4381 computer. The work was done while the first author (M.S.) was on sabbatical leave from the Universidad Nacional Autónoma de México in Mexico City.

## REFERENCES

1. J.-P. Caltagirone, Convection in a porous medium. In *Convective Transport and Instability Phenomena* (Edited by J. Zierep and H. Oertel), pp. 199–232. G. Braun, Karlsruhe (1982).
2. S. L. Moya, E. Ramos and M. Sen, Numerical study of natural convection in a tilted rectangular porous material, *Int. J. Heat Mass Transfer* **30,** 741–756 (1987).
3. P. Vasseur, M. G. Satish and L. Robillard, Natural convection in a thin inclined porous layer exposed to a constant heat flux, *Int. J. Heat Mass Transfer* **30,** 537–549 (1987).
4. J.-P. Caltagirone and S. Bories, Solutions and stability criteria of natural convective flow in an inclined porous layer, *J. Fluid Mech.* **155,** 267–287 (1985).
5. W. V. R. Malkus, Non-periodic convection at high and low Prandtl number, *Mém. Soc. Royale des Sciences de Liège*, 6e Série, Tome IV, pp. 125–128 (1972).
6. P. S. Damerell and R. J. Schoenhals, Flow in a toroidal thermosyphon with angular displacement of heated and cooled sections, *ASME J. Heat Transfer* **101,** 672–676 (1979).
7. J. E. Hart, A new analysis of a closed loop thermosyphon, *Int. J. Heat Mass Transfer* **27,** 125–136 (1984). See also J. E. Hart, A note on the loop thermosyphon with mixed boundary conditions, *Int. J. Heat Mass Transfer* **28,** 939–947 (1985).
8. M. Sen, E. Ramos and C. Treviño, On the steady-state velocity of the inclined toroidal thermosyphon, *ASME J. Heat Transfer* **107,** 974–977 (1985).
9. H. H. Bau and K. E. Torrance, On the stability and flow reversal of an asymmetrically heated open convection loop, *J. Fluid Mech.* **106,** 417–433 (1981).
10. R. Acosta, M. Sen and E. Ramos, Single-phase natural circulation in a tilted square loop, *Wärme- und Stoffübertragung* (1987), in press.
11. J. P. Walch and B. Dulieu, Convection de Rayleigh-Bénard dans une cavité poreuse faiblement inclinée, *J. Phys.-Lett.* **43,** L103–L107 (1982).
12. P. Vasseur, L. Robillard and I. Anochiravani, Natural convection in a shallow porous cavity heated from the side with a uniform heat flux, *Chem. Engng Commun.* **46,** 129–146 (1986).
13. A. Bejan and C.-L. Tien, Natural convection in a horizontal porous layer subjected to an end-to-end temperature difference, *ASME J. Heat Transfer* **100,** 1991–1998 (1978).
14. K. L. Walker and G. M. Homsy, Convection in a porous cavity, *J. Fluid Mech.* **87,** 449–474 (1978).
15. A. Bejan, The boundary layer regime in a porous layer with uniform heat flux from the side, *Int. J. Heat Mass Transfer* **26,** 1339–1346 (1983).
16. D. A. Nield, Onset of thermohaline convection in a porous medium, *Water Resour. Res.* **4,** 553–560 (1968).
17. D. W. Peaceman and H. H. Rachford, The numerical solution of parabolic and elliptic difference equations, *J. SIAM* **3,** 28–41 (1955).
18. H. Osoe, K. Fujii, N. Lior and S. W. Churchill, Long rolls generated by natural convection in an inclined rectangular enclosure, *Int. J. Heat Mass Transfer* **26,** 1427–1438 (1983).

## APPENDIX

Since we have not found in the literature a linear stability analysis of the vertical porous layer with end wall heating (Fig. 1(b) with $\phi = 0°$), we include a brief outline here. The problem is self adjoint so that the principle of exchange of stability holds. The time derivative in the governing equations can be eliminated and the linearized local form of equations (3) and (29) for small perturbations about the conductive state are

$$\nabla^2 T' = -\frac{\partial \psi'}{\partial y} \tag{A1}$$

$$\nabla^2\psi' = R\frac{\partial T'}{\partial y} \tag{A2}$$

where the primes indicate perturbations from steady-state values. $\psi'$ can be eliminated from these equations to give

$$\nabla^4 T' = -R\frac{\partial^2 T'}{\partial y^2}. \tag{A3}$$

The boundary conditions in the $y$-direction are

$$\psi' = 0, \quad \frac{\partial T'}{\partial y} = 0 \quad \text{at} \quad y = \pm\tfrac{1}{2}. \tag{A4}$$

The following normal forms

$$T' = T_0 \cos(mx)\sin(n\pi y) \tag{A5}$$

$$\psi' = \psi_0 \cos(mx)\cos(n\pi y) \tag{A6}$$

with $n = 1, 3, 5, \ldots$ satisfies equation (A1) and boundary conditions (A4). The wave number in the $x$-direction is represented by $m$. Substituting in equation (A3), we get

$$R = \frac{(m^2+n^2\pi^2)^2}{n^2\pi^2}. \tag{A7}$$

The least value of this is then

$$R_c = \inf_{\substack{m \text{ integer} \\ n = 1, 3, 5, \ldots}} \{R\} = \pi^2 \tag{A8}$$

for $n = 1$ and $m = 0$.

## ETATS STATIONNAIRES MULTIPLES DE LA CONVECTION NATURELLE UNICELLULAIRE DANS UNE COUCHE POREUSE INCLINEE

**Résumé**—On étudie la multiplicité des états stationnaires de la convection naturelle dans un matériau poreux incliné avec des isothermes parallèles conductives. Les différents états stationnaires sont obtenus analytiquement pour la convection unicellulaire dans des couches minces, rectangulaires, poreuses avec chauffage et refroidissement uniformes sur les parois opposées. La base de l'approximation analytique est une hypothèse d'écoulement parallèle sur une large portion de la couche. Les deux cas de flux thermique à travers les parois latérales et d'extrémités sont calculés et ils distinguent quelques configurations qualitativement semblables. Aux nombres de Rayleigh élevés et pour les inclinaisons suffisamment faibles, il existe des états instationnaires multiples dont quelques uns sont instables. On présente aussi une confirmation numérique des résultats analytiques stables.

## MEHRFACH STATIONÄRE ZUSTÄNDE BEI MONOZELLULARER NATÜRLICHER KONVEKTION IN EINER GENEIGTEN PORÖSEN SCHICHT

**Zusammenfassung**—Mehrfach stationäre Zustände bei der natürlichen Konvektion in einem geneigten porösen Material mit parallelen, gut leitenden Begrenzungen wird untersucht. Die verschiedenen stationären Zustände werden analytisch aus der monozellularen Konvektion in dünnen, rechteckigen porösen Schichten mit einheitlicher Heizung und Kühlung an gegenüberliegenden Wänden bestimmt. Grundlage der analytischen Näherung ist die Annahme paralleler Strömung über einen weiten Bereich der Schicht. Die Wärmeströme durch Seiten- und Endflächen werden jeweils berechnet, sie sind qualitativ ähnlich. Für unterkritische Rayleigh-Zahlen existiert für jeden Neigungswinkel nur je ein stationärer Zustand. Bei höheren Rayleigh-Zahlen und ausreichend kleinen Neigungswinkeln existieren beim Beheizen von unten mehrere stationäre Zustände, von denen einige instabil sind. Numerische Rechnungen, die die stabilen analytischen Berechnungen bestätigen, werden gezeigt.

## РАЗЛИЧНЫЕ СТАЦИОНАРНЫЕ РЕЖИМЫ ОДНОЯЧЕИСТОЙ ЕСТЕСТВЕННОЙ КОНВЕКЦИИ В НАКЛОННОМ ПОРИСТОМ СЛОЕ

**Аннотация**—Изучается многообразие стационарных режимов естественной конвекции в наклонном пористом слое с параллельными изотермическими теплопроводными границами. Аналитически получены различные стационарные режимы одноячеистой конвекции в тонких прямоугольных пористых слоях при равномерном нагреве и охлаждении противоположных границ. Аналитическое решение получено в предположении о наличии параллельного течения на большей части слоя. Рассчитаны два случая тепловых потоков через боковые и торцевые стенки, которые проявили общие качественные характеристики. Показано, что при докритических числах Рэлея и любом угле наклона слоя существует лишь одно стационарное состояние. Однако, при более высоких числах Рэлея и достаточно малых углах наклона нижней нагреваемой стенки наблюдались несколько стационарных режимов, некоторые из которых неустойчивы. Для устойчивых режимов полученные численные результаты подтверждают аналитические.